10/6-14-95 JS (1)

LBL-37028
UC-109

Center for Advanced Materials

CAM

Fundamental Studies of the Mechanism of Catalytic Reactions with Catalysts Effective in the Gasification of Carbon Solids and the Oxidative Coupling of Methane

Quarterly Report

October 1–December 31, 1994

E. Iglesia, D.L. Perry, and H. Heinemann

December 1994

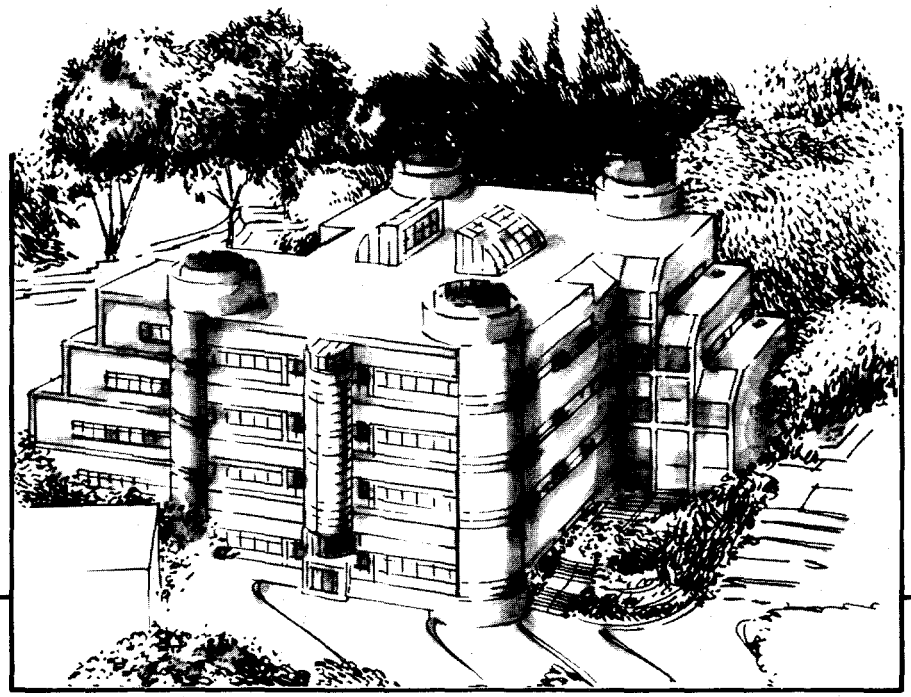

Materials and Chemical Sciences Division

Lawrence Berkeley Laboratory • University of California

ONE CYCLOTRON ROAD, BERKELEY, CA 94720 • (415) 486-4755

DISTRIBUTION OF THIS DOCUMENT IS UNLIMITED

Prepared for the U.S. Department of Energy under Contract DE-AC03-76SF00098

DISCLAIMER

This document was prepared as an account of work sponsored by the United States Government. Neither the United States Government nor any agency thereof, nor The Regents of the University of California, nor any of their employees, makes any warranty, express or implied, or assumes any legal liability or responsibility for the accuracy, completeness, or usefulness of any information, apparatus, product, or process disclosed, or represents that its use would not infringe privately owned rights. Reference herein to any specific commercial product, process, or service by its trade name, trademark, manufacturer, or otherwise, does not necessarily constitute or imply its endorsement, recommendation, or favoring by the United States Government or any agency thereof, or The Regents of the University of California. The views and opinions of authors expressed herein do not necessarily state or reflect those of the United States Government or any agency thereof or The Regents of the University of California and shall not be used for advertising or product endorsement purposes.

This report has been reproduced directly from the best available copy.

Available to DOE and DOE Contractors
from the Office of Scientific and Technical Information
P.O. Box 62, Oak Ridge, TN 37831
Prices available from (615) 576-8401

Available to the public from the
National Technical Information Service
U.S. Department of Commerce
5285 Port Royal Road, Springfield, VA 22161

Lawrence Berkeley Laboratory is an equal opportunity employer.

QUARTERLY REPORT

October 1, 1994 to December 31, 1994

FUNDAMENTAL STUDIES OF THE MECHANISM OF CATALYTIC REACTIONS WITH CATALYSTS EFFECTIVE IN THE GASIFICATION OF CARBON SOLIDS AND THE OXIDATIVE COUPLING OF METHANE

Principal Investigators: Enrique Iglesia
Dale L. Perry
Heinz Heinemann

Center for Advanced Materials
Materials Science Division
Lawrence Berkeley Laboratory
University of California
Berkeley, CA 94720

This work was supported by the Assistant Secretary for Fossil Energy, Office of Technical Coordination, U.S. Department of Energy under Contract DE-AC03-76SF00098, through the Morgantown Energy Technology Center, Morgantown, West Virginia 26505.

DISTRIBUTION OF THIS DOCUMENT IS UNLIMITED

MASTER

DISCLAIMER

Portions of this document may be illegible in electronic image products. Images are produced from the best available original document.

TABLE OF CONTENTS

I. Task Description for FY1995

II. Introduction

III. Highlights

a) *Oxidative Coupling of Methane*

b) *Synthesis and Characterization of Catalysts*

IV. Progress of Studies

a) *Oxidative Coupling of Methane*

b) *Synthesis and Characterization of Catalysts*

ATTACHMENTS:

I. **Extended Abstract** - Plenary Lecture, International Natural Gas Conversion Symposium, Johannesburg, Republic of South Africa, *"Reaction-Separation Schemes for C_2 Yield Improvements in the Oxidative Coupling of Methane"*

II. **Publication** - *Journal of Materials Research* **9** (11) 2993 (1994), *"Magnetic Characterization of Calcium-Nickel-Potassium Oxide Catalysts"*

III. **Extended Abstract** - 1994 Fall Meeting of the Materials Research Society, Boston, MA, *"Studies of Calcium-Nickel-Potassium Oxide Films by Synchrotron X-Ray Fluorescence Microscopy"*

I. Task Descriptions for FY 1995

Task 1 - *Oxidative Methane Coupling: Reaction-Separation Processes for Methane Conversion to Ethane and Ethylene*(E. Iglesia and H. Heinemann, Principal Investigators)

The synthesis of ethane and ethylene from methane and oxygen will be carried out in novel hydrogen transport inorganic membranes and in cyclic reactors in order to prevent undesirable secondary reactions of C_2 molecules to CO and CO_2. Neither inorganic membrane reactors nor cyclic tubular reactors are presently used in commercial processes. Their application to catalytic reactions represents a novel application of engineering and solid-state chemistry concepts to catalytic reactions.

Our approach combines high temperature membrane and cyclic experimental reactors, synthesis and characterization of thin membrane films and of high surface area catalysts, and detailed models of complex gas phase and surface reactions involved in oxidative coupling. We anticipate that this approach will lead to novel reactors for carrying our kinetic-controlled sequential reactions, such as the oxidative coupling of methane.

Task 2 - *Synthesis and Characterization of Catalysts* (D.L. Perry, Principal Investigator)

Careful spectrographic and wet chemical analyses of fresh and spent catalysts have shown considerable differences which have permitted conclusions as to the source of deactivation; this work will be continued in fiscal 1995

II. Introduction

Our activities in the first quarter FY1995 have focused on the synthesis, structural characterization, and catalytic evaluation of membrane films, disks, and reactors. We have also continued to exploit reaction-transport models to predict the performance of membrane, cyclic, and recycle reactors in the oxidative coupling of methane.

A graduate student (Richard W. Borry) and a post-doctoral fellow (Dr. Srinivasan Sundararajan) were assigned full-time to the project during the quarter. Both the cyclic

and membrane reactors are operational but the work during this quarter has concentrated on perovskite materials in membrane reactor configurations.

III. Highlights

Our experimental and theoretical studies of the selective activation of methane using reaction-separation reactor schemes were described in an extended abstract submitted as a plenary lecture for the 1995 International Natural Gas Conversion Symposium. (Attachment I: *"Reaction-Separation Schemes for C_2 Yield Improvements in the Oxidative Coupling of Methane"*). Experimental characterization work on Ca-Ni-K oxides has recently appeared in the *Journal of Materials Research* (Attachment II: *"Magnetic Characterization of Calcium-Nickel-Potassium Oxide Catalysts")* and as an extended abstract at the 1994 Fall Meeting of the Materials Research Society (Attachment III: *"Studies of Calcium-Nickel-Potassium Oxide Films by Synchrotron X-Ray Fluorescence Microscopy")*

a) Oxidative Methane Coupling

- Methane pyrolysis reactions have been carried out in a steady-state flow reactor without catalyst at 800, 900, and 1000 °C in order to examine the behavior of the gas phase pyrolysis reactions in the methane side of the membrane reactor Trace amounts of ethane and ethylene were formed at 800 °C in an empty reactor. At 900 °C, methane conversion was 6.0%, with ethylene, acetylene and aromatic hydrocarbons and solid carbon (coke) the major products. At 1000 °C, 23.7% of the entering methane was converted to aromatics and coke and 6.4% was converted to C_2 hydrocarbons.

- The results of the pyrolysis experiments and thermodynamic calculations indicate the need to maintain the temperature of the methane reaction below 800 °C in order to prevent coke formation. A detailed kinetic model for free radical methane pyrolysis is being developed in order to describe these data and to predict the temperature and concentration range required to minimize carbon formation.

- A controlled pH co-precipitation unit has been designed and tested. Intimately mixed powders of any desired stoichiometry can now be prepared in a controlled and reproducible manner. These will be used as precursors for membrane films supported on inorganic porous substrates. Several sources of these porous substrates have been identified for the formation of films by coating or pulsed laser deposition studies.

- Interstage C_2 removal in multi-stage tubular reactors has been examined using a modified version of our oxidative coupling kinetic-reactor models. The effect of separation efficiency on attainable C_2 yields has been quantified.

c) Synthesis and Characterization of Catalysts

- A paper describing the variation in the magnetochemistry of the Ni-Ca-K oxide catalysts in powdered form has appeared in the *Journal of Materials Research* and is included in the Appendix of this report

- Some of the results of the synchrotron fluorescence data have been presented at the 1994 Fall Meeting of the Materials Research Society, Boston, MA, and a preprint of the refereed proceedings contribution is included in the Appendix of this report

- Initial experimental approaches for the preparation of the diffusion membrane films involve the use of porous, fritted ceramic, high temperature supports onto which diffusion membranes consisting of Sr-Zr-Y oxide are placed; earlier experimental results showed that the films could be fabricated on solid supports.

IV. Progress of Studies

a) Oxidative Coupling of Methane

Methane Pyrolysis Experimental Results

Methane was reacted at high temperature in an empty quartz/alumina flow reactor at 1 bar total pressure. The inlet gas composition was Ar:CH_4:He (1:1:13.5 vol.). This stream consisted of an Ar-CH_4 mixture (50.00:50.00 ± 0.02%) combined with pure He (99.9995% purity). The individual flow rates were controlled with Porter mass flow controllers at a total rate of 34.9 ml/min. The reactor volumetric space velocity was 2.7 min^{-1}.

The gas stream exiting the reactor was sampled automatically using an automated sampling valve and the collected samples were injected into a Carboxen 1000 packed column (5' x 1/8" 45/60 mesh, Supelco, Inc.) in a Perkin Elmer Sigma 2000 GC. Thermal conductivity and flame ionization detector response data were analyzed using a HP Chemstation. Argon was the internal standard for all runs. Steady-state was achieved within 30 minutes, as indicated by three consecutive samples with concentrations variations less than 2 %.

The data in Figure 1 are reported as the average of three consecutive steady-state samples at each temperature. The coke yield was obtained from a carbon balance (+/-5 %). Substantial carbon deposition was clearly visible on the reactor walls after the 1000°C experiment. These results show that methane pyrolysis reactions require low temperatures and/or short residence times for high C_2 selectivity. Methane conversions, however, are low at these conditions for gas phase pyrolysis reactions. Therefore, the surface of proton-transport membranes (or of an appropriate coating) must act as methane pyrolysis catalysts and lower the high temperatures required in the absence of a catalyst. Catalytic pyrolysis has not been examined in detail in previous literature reports because pyrolysis thermodynamics are unfavorable at such low temperatures. This restriction disappears as one of the reaction products (H) is removed in our proton-conducting membrane configuration.

Figure 1: Products of Methane Pyrolysis in a Flow Reactor

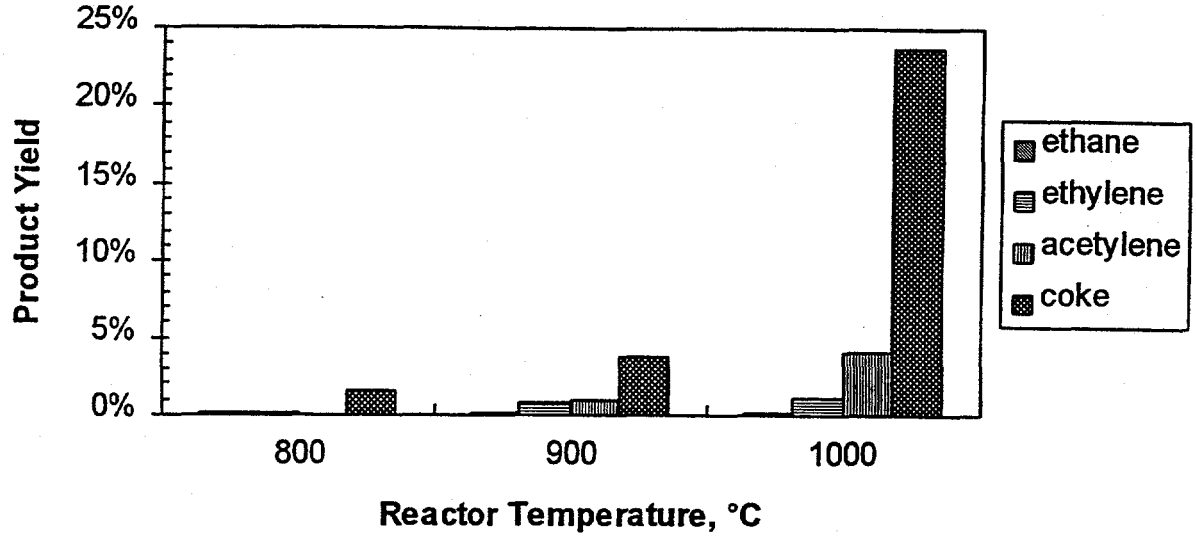

Methane conversion was 2.3, 6.0, 30.1% at 800, 900, 1000 °C, respectively.

Methane pyrolysis chemistry proceeds via free radicals and methyl radicals are usually the predominant radical species. The reaction proceeds sequentially by chain growth from methyl radicals to ethane, then ethylene, acetylene, and cyclic and aromatic carbon species and coke. The question then arises, if a suitable catalyst can be found to increase the initial reactions (involving C_2 products), what would be the thermodynamic equilibrium distribution? That is, if the catalytic surface just forms free radicals more rapidly than gas phase reactions, the final product distribution will ultimately reflect the same thermodynamic equilibrium as in the gas phase reaction. This equilibrium can be shifted towards C_2 products by the continuous removal of hydrogen across a proton-conducting membrane.

Table 1 presents the calculated thermodynamic equilibrium compositions of the inlet gas stream used in the experiments of Figure 1, assuming the only products to be ethane, ethylene, and acetylene. The first column represents conventional reaction conditions, while the second and third present the results obtained when hydrogen is removed continuously from the reactor, as in proton conducting membrane reactors.

Table 1: Thermodynamic Equilibrium of CH_4, C_2H_6, C_2H_4, C_2H_2 With and Without Hydrogen Removal.

	No H_2 removed		1 mole H_2 per mole CH_4 in the feed removed		2 moles H_2 per mole CH_4 in the feed removed	
°C	CH_4 % conversion	C_2H_4 % yield	CH_4 % conversion	C_2H_4 % yield	CH_4 % conversion	C_2H_4 % yield
600	3.7	3.2	47.0	38.9	83.3	49.2
800	20.4	13.1	48.8	23.0	77.5	22.2
900	38.2	14.9	59.3	16.9	81.4	13.8

Figure 1 shows that these membrane reactors must operate below 900 °C in order to minimize carbon formation. Our target operating temperatures are 600-700 °C, a challenge that requires that we increase the proton conductivity or decrease significantly the thickness of available proton-conducting membranes. In a steady-state flow reactor without hydrogen removal, this low temperature would limit methane conversion to 3.7%. However, if one hydrogen atom per methane molecule can be removed from the reactor during the course of reaction, the methane conversion increases to 47%, with a 39% yield of ethylene. This would be a dramatic improvement over existing conventional oxidative coupling processes.

The next series of pyrolysis experiments will look at heterogeneous reaction at temperatures in the range of 600-900 °C, using the known hydrogen conducting perovskite materials in powder form and then in membrane morphologies.

Controlled pH Co-Precipitation Unit

In order to prepare the required thin non-porous hydrogen transport membranes, we must be able to prepare intimately mixed powders with stoichiometric $SrCe_{0.9}Yb_{0.1}O_{3-\delta}$ composition and high phase purity. Intimate mixing of the three cations is needed to form the perovskite structure, while a fine powder size is needed to form dense membranes by spin coating, casting, and controlled sintering techniques.

Currently, we use a ceramic method to prepare these perovskite powders. This involves physical mixing of precursor powders ($SrCO_3$, CeO_2, Yb_2O_3) in the solid-state, followed by high temperature calcination (800°C in air) to form the oxides, and a very high temperature (1500°C) sintering stage in order to form intimately mixed pure perovskites. The resulting membranes are limited to disks of 1 mm minimum thickness because of mechanical integrity during cutting, mounting, and high temperature reactor operation.

Similar perovskite materials are being prepared chemically for thin film applications in the high temperature superconductor field. One such technique is to precipitate insoluble hydroxides of the precursor cations. Nitrate and acetate salts of Sr^{2+}, Ce^{3+} and Yb^{3+} readily dissolve in deionized water. In solution, the cations are mobile and mix completely. At a pH value greater than 6, the cations form hydroxide salts ($Sr(OH)_2$, $Ce(OH)_3$, and $Yb(OH)_3$) which are insoluble in water and precipitate from solution.

During 1Q'FY1995, we have designed and tested a controlled pH precipitation unit that allows the co-precipitation of these insoluble hydroxides in a controlled and reproducible manner. This unit is shown schematically in Figure 2. The metal salts are dissolved in deionized water in the stoichiometric ratio of the desired perovskite. These are added to the reaction vessel at a constant rate, which is slow enough so that the reaction mixture is completely mixed at all times. A meter reads the pH of the solution and feeds the information to computer control software that in turn sends a signal to a pump that feeds a basic solution at a rate sufficient to maintain a constant pH in the reaction vessel. Nitrogen is bubbled through the solution to exclude dissolved CO_2 (as carbonic acid) and O_2 from the reaction mixture. A thermocouple records the temperature of the solution, which can be adjusted by changing the temperature of the heating jacket around the solution vessel.

Figure 2: Controlled pH Co-Precipitation Unit

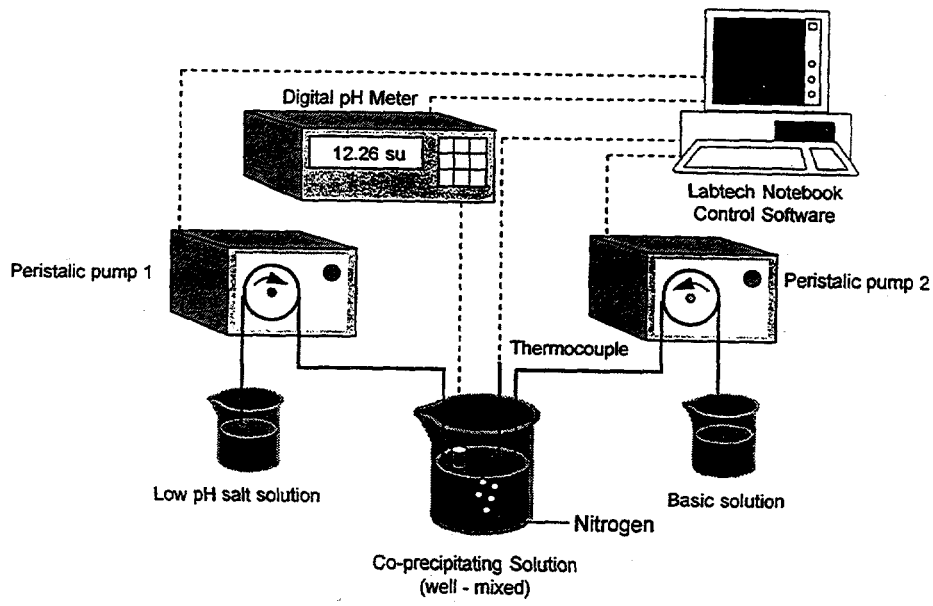

This unit will be used to prepare homogenous fine powders of the desired perovskite structures. These powders will then be calcined to remove the basic anions and finally pressed and sintered to form the dense perovskite structures for use in membrane experiments. Previous experience in the high temperature superconductor field has shown this method to produce very dense samples, and allows lower sintering temperatures than those required by the ceramic method.

During this quarter, we have gained access to x-ray diffraction software in order to perform structure refinements on perovskite diffraction patterns and ascertain the phase purity of the resulting materials.

Simulations of Tubular Reactors with Interstage C_2 Removal

The effect of C_2 removal efficiency on the maximum C_2 yields attained in tubular reactors with interstage C_2 removal was examined using kinetic-reactor models for homogeneous-heterogeneous coupled oxidative coupling pathways in tubular reactors. The results of these simulations are shown in Figure 3. For 10 removal stages, maximum C_2 yields are above 50 % for removal efficiencies of 100% but C_2 yields decrease to about 35% when only 50% of the ethane/ethylene is removed in each interstage separation step. In the latter case, about 25 interstage separators are required to obtain 50% C_2 yields.

Our next extension will introduce into the simulation code specific separation processes in an interstage separator or within a recycle stream in tubular recycle reactors. Specifically, we will examine the use of high-temperature Knudsen diffusion porous membranes for the selective removal of unreacted methane and the use of absorbents and of capillary condensation within microporous solids for partial C_2 removal near room temperature. Both of these approaches would decrease significantly the separation and energy costs associated with recycle and cryogenic distillation processes for C_2 removal.

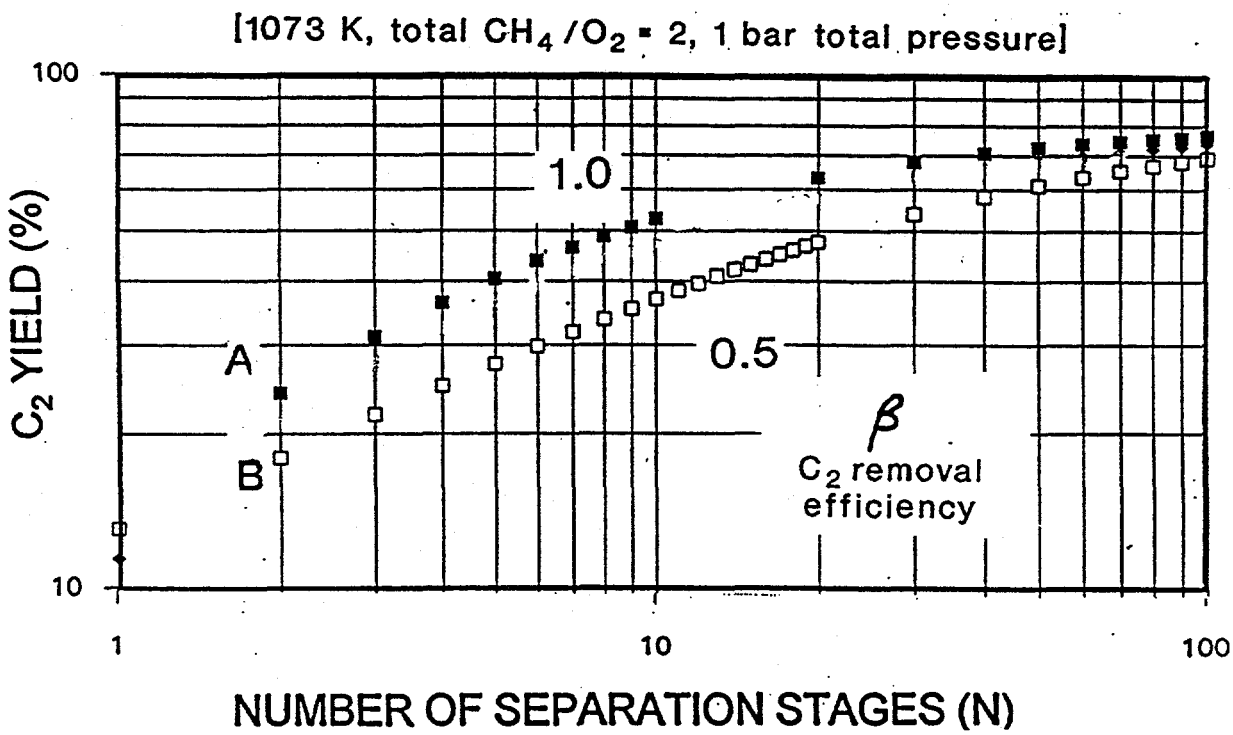

Figure 3. Simulated Effect of Interstage C_2 Removal Efficiency on C_2 Yields

Cyclic Reactors for Oxidative Coupling

We completed early in this quarter the mechanical troubleshooting of the unit and we have replaced a failing furnace with another existing one. We have been unable to operate the mass spectrometer reliably for any significant period of time. No cyclic methane decomposition experiments were run during the quarter because of these problems. We consider additional time and budget expenditures in repairing this mass spectrometer to be counterproductive. We are presently looking into the availability of alternate spectrometers at LBL and also exploring any opportunities for the purchase of a new spectrometer in the next few months. In the meantime, we have shifted all resources into the membrane reactor and modeling efforts.

b) Synthesis and Characterization of Catalysts

Studies of Strontium-Zirconium-Yttrium Oxide Films and Membranes

Initial membranes of Sr-Zr-Y oxide have been fabricated using pulsed laser deposition techniques and Y-stabilized zirconia as the substrate. The target composition for these studies was $SrZr_{0.9}Y_{0.1}O$. X-Ray diffraction lines attributable to the target composition phase were identified based on previous data from our laboratory. Other target/membrane compositions that have been fabricated include: Ce-Sr-Y oxide systems with stoichiometries similar to those of the Sr-Zr-Y system presently being studied as a fast proton conductor. These stoichiometries will be further studied as ablated films. Variations in porosity involving the substrate onto which the film is ablated are also being studied.

X-Ray Fluorescence Microprobe Studies on Ca-Ni-K Films

Continued studies of calcium-nickel-potassium films using the x-ray fluorescence microprobe approach have been conducted at the Advanced Light Source synchrotron facility at the Lawrence Berkeley Laboratory. Emphasis has been placed on studying the degree of heterogeneity with respect to the calcium, nickel, and potassium in the film matrices. The films have been fabricated in a wide range of stoichiometries in order to show that the films (coatings) can be experimentally ordered with respect to different,

desired compositions. Studies of these films have also been made using x-ray diffraction to document the various phases that have been made, including new ones that have been heretofore unreported. Energy dispersive x-ray spectroscopy has been used to obtain stoichiometries. A manuscript describing the x-ray synchrotron results will be prepared for submission to a journal.

ATTACHMENTS

I. **Extended Abstract** - Plenary Lecture, International Natural Gas Conversion Symposium, Johannesburg, Republic of South Africa, *"Reaction-Separation Schemes for C_2 Yield Improvements in the Oxidative Coupling of Methane"*

REACTION-SEPARATION SCHEMES FOR C_2 YIELD IMPROVEMENTS IN THE OXIDATIVE COUPLING OF METHANE

E. Iglesia, R.W. Borry, and S.C. Reyes[1]
Department of Chemical Engineering, University of California at Berkeley, Berkeley, CA 94720 and [1]Corporate Research Laboratories, Exxon Research and Engineering, Route 22 East, Annandale, NJ

Ethane and ethylene yields in the oxidative coupling of methane are currently limited by their subsequent oxidation to CO and CO_2. Higher C_2 yields will require catalytic solids that activate CH_4 but not C_2 hydrocarbons, which appears improbable at this time. Our research addresses the mechanistic and practical implications of alternate approaches to increase C_2 yields in this reaction. Our strategy minimizes the contact between the O_2 reactant required for favorable thermodynamics and the C_2 products of the coupling reaction. It combines detailed kinetic-transport models with experimental demonstration of the reaction-separation schemes suggested by the model simulations.

We have developed and used reaction-transport models that combine detailed gas phase and surface kinetic networks with rigorous descriptions of convective and diffusive transport processes within catalytic reactors, pellets, and membranes. We exploit these models to examine the behavior of several reaction-separation schemes:

i) staged oxygen feed tubular reactors and oxygen transport membranes
ii) tubular flow reactors with interstage separation of ethane and/or ethylene
iii) recycle reactors with ethane and/or ethylene separation in recycle stream
iv) catalytic hydrogen transport membranes
v) sequential methane decomposition and hydrogen oxidation cyclic reactors

Our simulations suggest that distributed injection of O_2 or C_2 removal along tubular reactors increase C_2 yields by inhibiting homogeneous C_2 oxidation pathways. Oxygen distribution by sequential injection or by oxygen membranes, however, decreases methyl radical generation rates. C_2 yields are limited to about 30 % and large volumes are required for staged feed reactors. In contrast, C_2 product removal between stages or from recycle streams inhibits oxidation to CO_x without decreasing methane activation rates. C_2 yields above 50 % can be achieved using modest methane conversions per stage (10%) (Figure 1) and recycle ratios (20) (Figure 2). As the number of stages increases, C_2 yields approach 90%; this limit is imposed by the rate of direct oxidation of CH_4 to CO_x on catalytic sites, a process that is not influenced by C_2 removal.

Hydrogen transport membranes maintain hydrocarbons and oxygen streams separate and permit the use of air instead of O_2 as the oxidant. On one side, CH_4 undergoes catalyst-initiated pyrolysis; the H-atoms formed diffuse across the membrane and react with O_2 in the opposite side in order to provide the required thermodynamic driving force for the reaction (Figure 3). Similar effects are obtained by operating a tubular reactor using two cycles: a methane cycle where CH_4 is activated and the H-

atoms diffuse into the solid and an oxidation cycle in which O_2 reacts with absorbed H-atoms (Figure 4). Our simulations combine kinetic descriptions of thermal and catalytic pyrolysis reactions with steady-state diffusion across proton-conducting transport membranes (Figure 3) or with transient H-formation, absorption, and scavenging in cyclic reactors (Figure 4). Our experimental studies explore the relative efficiency of these two approaches and the design of hydrogen transport membranes and cyclic reactors to improve C_2 yields in the conversion of methane to higher hydrocarbons.

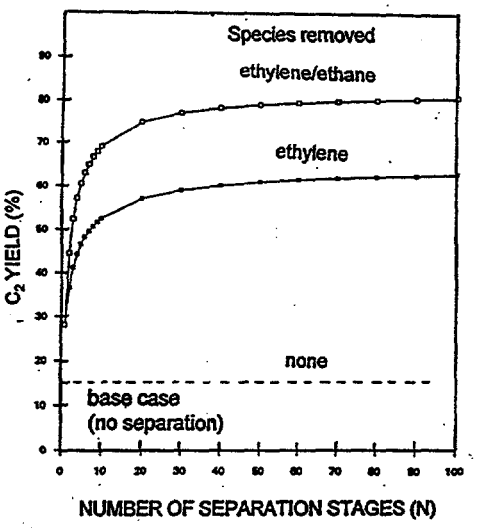

e 1. Maximum C_2 yields in co-feed tubular reactors with interstage C_2 removal (Model simulations, 1073 K, inlet CH_4/O_2=2, 1 bar)

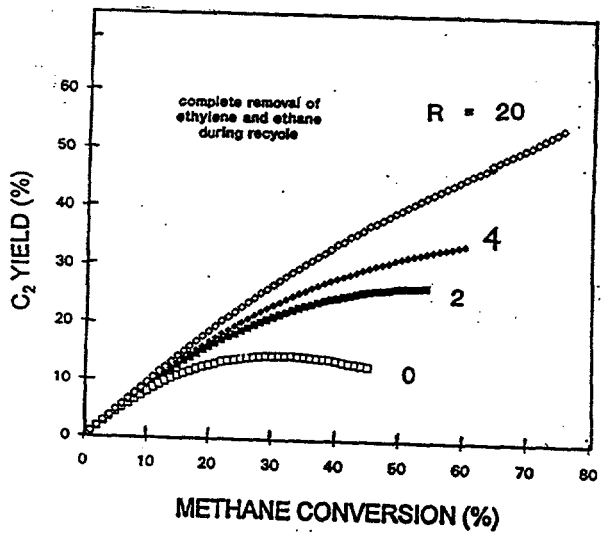

Figure 2. C_2 yields in co-feed tubular reactor with C_2 removal from recycle stream (Model simulations, R= recycle ratio, 1073 K, inlet CH_4/O_2=2, 1 bar)

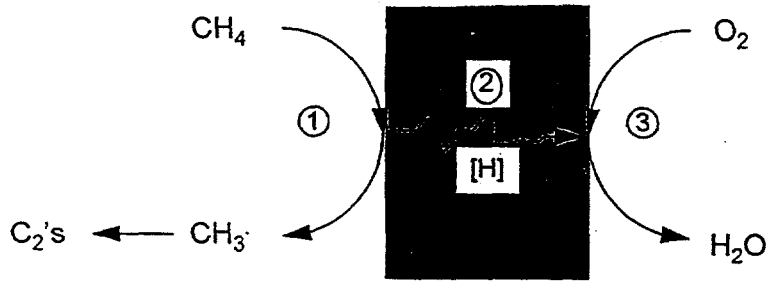

Figure 3. Coupled methane pyrolysis and hydrogen oxidation using proton-conducting oxide membranes

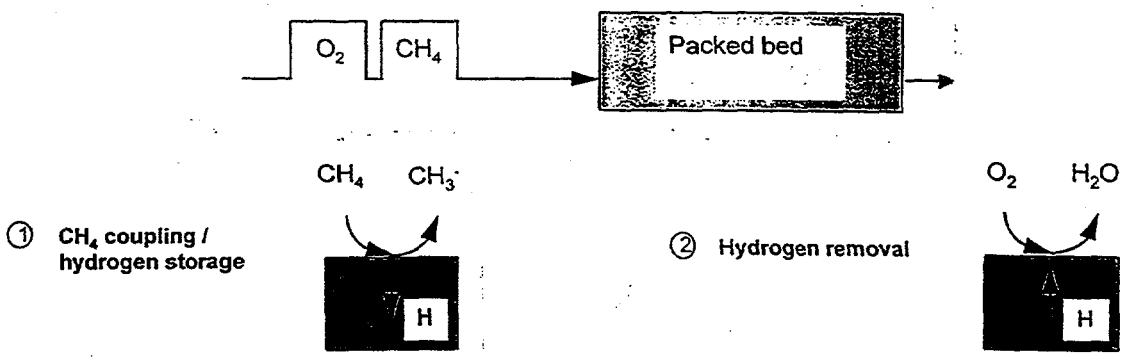

Figure 4. Sequential methane pyrolysis and hydrogen oxidation using cyclic fixed-bed reactor

II. **Publication** - *Journal of Materials Research* **9** (11) 2993 (1994), *"Magnetic Characterization of Calcium-Nickel-Potassium Oxide Catalysts"*

Magnetic characterization of calcium-nickel-potassium oxide catalysts

Dale L. Perry,[a] Paul Berdahl, and Charles Perrino
Lawrence Berkeley Laboratory, Berkeley, California 94720

(Received 31 January 1994; accepted 22 July 1994)

SQUID magnetometer characterization of Ca–Ni–K–O catalyst materials reveals complex magnetic behavior. The magnetic properties are generally determined by the antiferromagnetic material NiO, but samples with traces of elemental nickel show marked effects of ferromagnetism. Potassium doping enhances the formation of metallic nickel. Further deviations from bulk NiO properties can be attributed to NiO particle size effects (superparamagnetism) and to the presence of paramagnetic impurities, possibly Ni^{3+} ions.

I. INTRODUCTION

Mixed metal oxides in the Ca–Ni–K–O system are active in the catalyzed gasification of carbonaceous materials.[1–6] In addition to having been synthesized as powders, they have also been fabricated as films.[7] The accurate characterization of these materials is complex due to their sensitivity to details of the processing conditions used to make them. The magnetic properties of these materials may be expected to depend primarily on the spin magnetic moments of the electrons in the partially filled $3d$ orbital of the nickel atoms and ions. Isolated Ni^{2+} and Ni^{3+} ions are expected to have spins of 1 and 3/2, and moments of about 2.8 and 3.9 Bohr magnetons, respectively. In metallic nickel the $3d$ orbitals overlap to form a band that is not quite full. The electrons in this band experience an exchange interaction that tends to align spins parallel to one another. Since the band is not full, there is a net density of parallel spins, leading to ferromagnetism, with a saturation moment of 0.6 Bohr magnetons per atom. The material NiO is an antiferromagnetic semiconductor. In this case the magnetic Ni^{2+} ions order antiferromagnetically below the Néel temperature (525 K) due to electronic interactions mediated by the oxygen atoms.

In the form of small particles, both nickel metal and nickel oxide exhibit the phenomenon of superparamagnetism. Consider the ferromagnetic case first. Small ferromagnetic particles below roughly 15 nm diameter contain only a single magnetic domain, due to the finite energy required to make a domain wall. The spontaneous moment can rotate freely if the temperature is high enough to overcome any energy anisotropy (due to stress, particle shape, crystal lattice, etc.). An assembly of such particles behaves thermally and magnetically just as though it were an ordinary paramagnetic material, but with a moment that is much larger than an atomic moment. The resulting magnetic behavior was named superparamagnetism by Bean.[8] Two important characteristics of superparamagnetism are the absence of magnetic hysteresis and, further, that the magnetic moment of the sample is a function of the ratio H/T only (field/temperature), after correcting for the temperature dependence of the moments of the individual particles. These superparamagnetic characteristics are seen only above the so-called blocking temperature (below which the effects of anisotropy are important). Provided that a sample is fully superparamagnetic, information on the size of the ferromagnetic particles can be deduced from the functional dependence of magnetization with field. Further information on superparamagnetic nickel particles may be found in the review by Jacobs and Bean[9] and in Refs. 10–14.

Superparamagnetism of small NiO particles was first observed by Richardson and Milligan.[15] They found that for particle sizes above roughly 100 nm, the magnetic properties were those expected[16] for an antiferromagnetic material; the magnetic susceptibility is almost independent of temperature, with a cusp at the Néel point (525 K). However, for particle sizes below 100 nm, the magnetic susceptibility increased greatly (paramagnetically) as the temperature is lowered, reaching a maximum of 25 times the bulk values at temperatures in the range of 100 to 200 K and decreasing below these temperatures. Superparamagnetism was initially difficult to explain in antiferromagnetic materials, because single domain particles might be expected to have zero spontaneous magnetic moment. The explanation was provided by Néel,[17,18] who pointed out that for small particles, the magnetization of the two antiferromagnetic sublattices is unlikely to cancel entirely; the uncompensated spins produce the particle's spontaneous moment. Further information on

[a]Author to whom correspondence should be addressed.

the superparamagnetic properties of small NiO particles may be found in the literature.[19–23]

II. EXPERIMENTAL

Six Ca–Ni–K–O samples (A through F) were selected for magnetic measurements. They were prepared by mixing molar ratios of 2 : 1 : 0.1 of the hydroxides of calcium, nickel, and potassium, respectively, except for Sample A, from which the potassium was omitted. Each sample was calcined in air. Samples A and B were treated identically, being heated at 735 °C for 3 h. A and B acquired carbon during processing as may be seen in the summary of x-ray diffraction results in Table I. The C : Ca ratio is nearly 1 : 1. Samples C, D, E, and F were fired in a furnace for times of 1, 2, 3, and 4 h, respectively, to final temperatures of 485, 690, 759, and 808 °C. Subsequent analysis of the metallic content of the samples showed the expected 2 : 1 ratio of calcium to nickel, but showed that potassium levels were reduced by the calcination process, with 1/4 of the potassium lost at the lowest temperature (485 °C) and 1/2 of the potassium lost at the highest temperature (808 °C).

The magnetic measurements were performed with a Quantum Design model MPMS SQUID magnetometer. (SQUID is an acronym for Superconducting QUantum Interference Device.) The static magnetic moment was measured over the temperature range 5 to 280 K and over the magnetic field range 0 to 40 kG (0 to 4 T). The usual procedure was to determine the magnetic moment while warming the sample from 5 K to 280 K in a field of 10 kG, followed by cooling back to 5 K in a field of 40 kG, and concluding by reducing the field from 40 kG to 0 at 5 K. The time for each individual moment determination was about 30 s. A correction was made for the diamagnetic plastic sample container, based on its measured moment.

III. RESULTS AND DISCUSSION

Samples A and B proved to be particularly magnetic, as shown in Fig. 1. The markedly nonlinear behavior of magnetic moment with field, saturating at fields below 10 kG, is suggestive of metallic nickel. The linear slope observed at the higher fields is attributed to the linear dependence of magnetization on field expected for antiferromagnetic NiO. The saturation moment decreases weakly with increasing temperature (not shown), which is also indicative of nickel. These results are in general agreement with prior work with powders containing fine nickel particles.[11,13] Based on the saturation moment of bulk nickel, the fraction of nickel that is present in the metallic form is estimated as 1.5% for sample A and 5% for sample B. Since samples A and B were prepared in identical fashion, except that B was doped with potassium, it appears that potassium assists the formation of Ni^0 in this case. The x-ray diffraction results shown in Fig. 2 exhibit small peaks for nickel, at precisely the location (44.5°) of the most intense diffraction peak in the nickel spectrum, confirming the presence of metallic nickel.

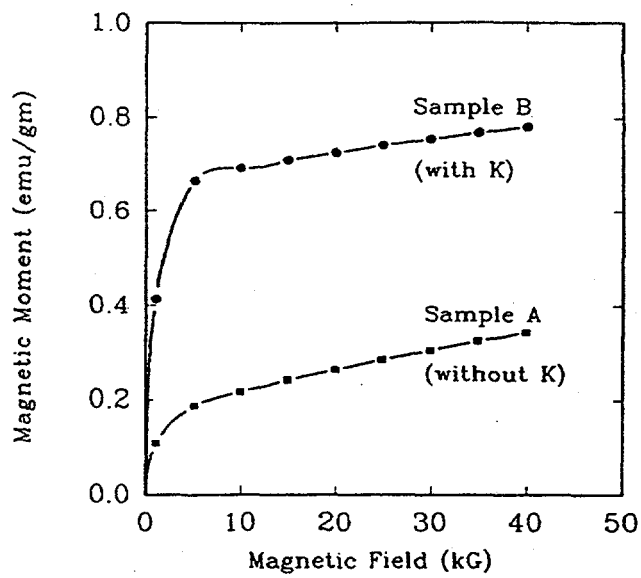

FIG. 1. Magnetic moment per unit mass as a function of applied field for two Ca–Ni–O samples at 5 K, with and without potassium doping.

The magnetic moment of the other four samples is shown in Fig. 3 as a function of field. In each case the plot is more nearly linear for these less magnetic samples. Sample C, which was calcined at relatively low temperatures, has an anomalously high moment compared with the other samples D, E, and F. This enhanced moment is attributed to the superparamagnetism of NiO particles smaller than 100 nm.[15,17–23] It is not seen in the other samples due to the higher processing temperature which promotes the growth of larger grains. The curvature in these plots is due to paramagnetic "impurities," possibly Ni^{3+} ions associated with excess oxygen, to be discussed below in connection with the temperature dependence at low temperatures. The large remnant moment of sample C can be identified with

TABLE I. Sample composition as determined from x-ray diffraction.

Sample	Dominant calcium phase	Other calcium phases	NiO	$Ni^{(O)}$
A	$CaCO_3$	CaO, $Ca(OH)_2$	Yes	Yes
B	$CaCO_3$	CaO, $Ca(OH)_2$	Yes	Yes
C	$Ca(OH)_2$	...	Yes	No
D	$Ca(OH)_2$	...	Yes	No
E	$Ca(OH)_2$	...	Yes	No
F	$Ca(OH)_2$	...	Yes	No
NiO	...	...	Yes	No

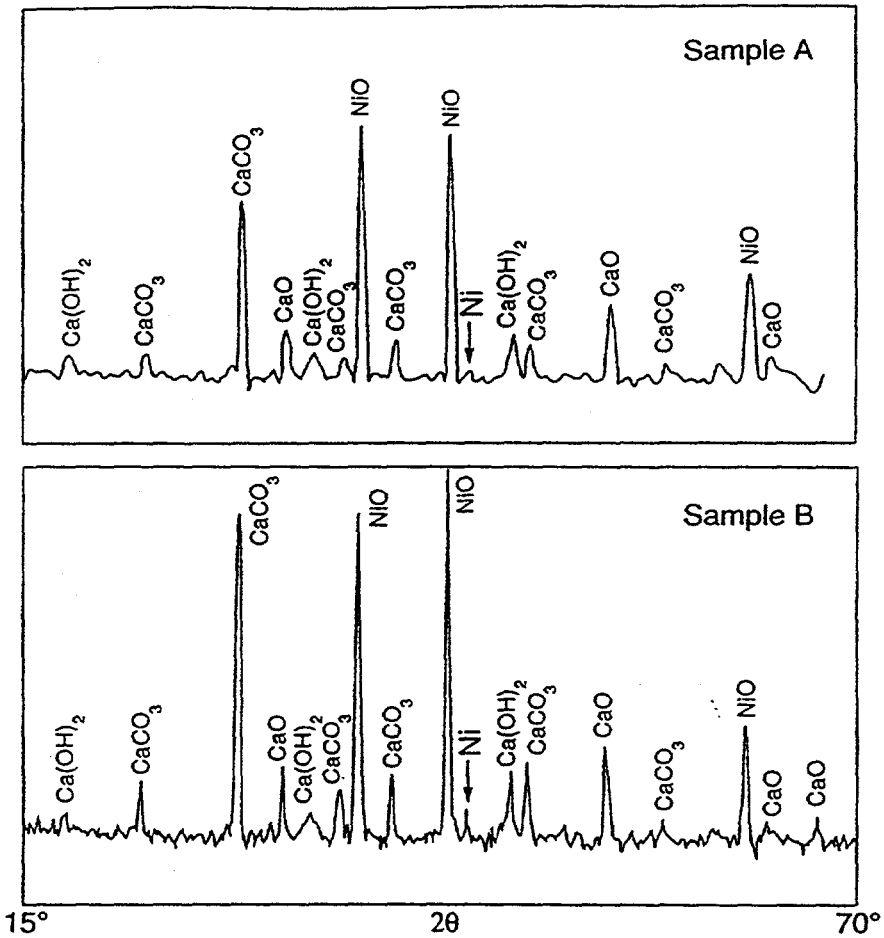

FIG. 2. X-ray diffraction data for samples A and B, showing the presence of small peaks for Ni^{O}.

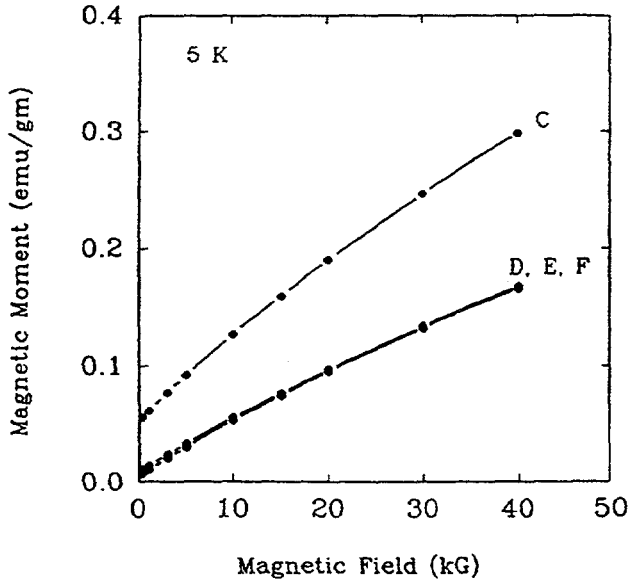

FIG. 3. Magnetic moment per unit mass as a function of applied field for samples C, D, E, and F, at 5 K.

the locking of the superparamagnetic moment below the blocking temperature.

Data at lower fields are shown for all six samples in Fig. 4. Note that the low-field behavior of the metal-containing samples A and B is qualitatively different from that of the other samples, a fact which is useful in detection of Ni^{O} in oxide mixtures. Sample C has the largest remnant moment, 0.055 emu/gm. If this remnant moment were due to nickel metal, the fraction of nickel in the metallic form would be roughly 0.3%, too small to be readily detected by x-ray diffraction. The more magnetic samples A and B show rather small remnant moments (only a few percent of the saturation moments), even at 5 K. For superparamagnetic nickel particles, one may expect that the blocking temperature is above 5 K, and that therefore the remnant moment should be larger. For example, Gittleman *et al.*[10] give blocking temperatures of 20 K for 4 nm particles and show a trend toward smaller blocking temperatures for smaller particles. However, the existence of a sharp x-ray diffraction peak shows that some of the particles must be at least a few nanometers in size. To summarize, the remnant moments for samples A and B show that

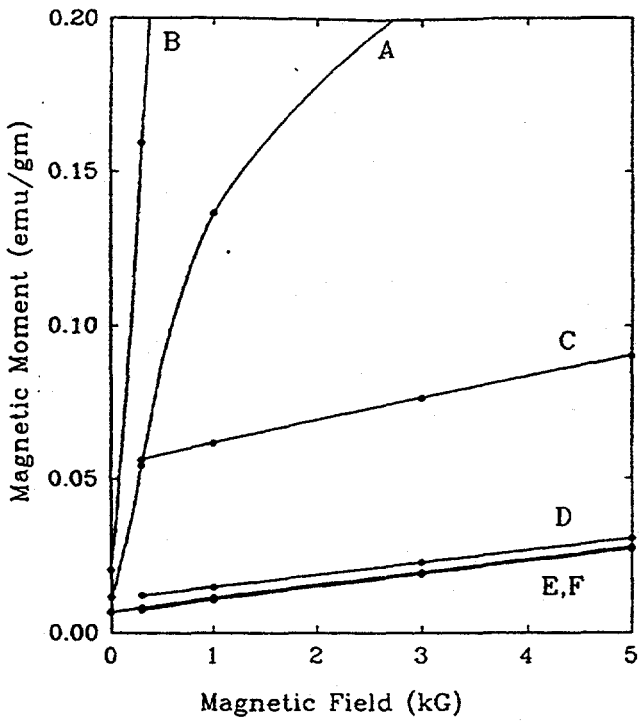

FIG. 4. Magnetic moment of all Ca–Ni–O samples at lower fields, at 5 K.

most of the moment associated with elemental nickel is not aligned at 5 K and zero field, presumably due to thermal agitation. While this observation is puzzling, it is in agreement with prior observations on some samples with small nickel particles.[24]

Figure 5 shows the temperature dependence of the moment of NiO reagent powder and samples C, D, and F. The data for NiO have been scaled as though the NiO had been diluted (3.04 : 1 by weight) by nonmagnetic $Ca(OH)_2$, for comparison with the other samples. Table II gives numerical results at 280 K and 40 kG for all samples. The measurement for NiO corresponds to a magnetic susceptibility of 1.18×10^{-5} emu gm^{-1} Oe^{-1} at 280 K, which may be compared with 9 to 9.5×10^{-6} for large particles of NiO and single crystals.[15,16,22] According to Richardson *et al.*,[22] the room temperature value of the susceptibility increases with decreasing particle size in a systematic way. Our susceptibility value for the NiO reagent powder then corresponds to roughly 100 nm particle size. Then samples D, E, and F have larger particle sizes and sample C, smaller sizes.

The superparamagnetism of NiO in sample C is indicated by the enhanced magnetic moment and increased temperature dependence of the moment. However, the detailed dependence differs from that observed in measurements of pure NiO particles.[15] One possible explanation for the temperature dependence observed in Fig. 5 may be the presence of a small quantity of very small (10 nm) particles in sample C.

All samples exhibit the presence of paramagnetic "impurities" due to the upturn in magnetic moment below 50 K. A plausible explanation for this upturn is the presence of a small quantity of Ni^{3+} ions in NiO. The black color of reagent NiO is generally attributed to Ni^{3+} ions associated with excess oxygen, and the grey color of the Ca–Ni–K–O samples investigated here may well have this origin as well. The concentration of these presumed Ni^{3+} ions can be estimated based on the magnitude of the low temperature peaks in Fig. 5, using Curie's law. It may also be estimated from the curvature in Fig. 3, by attributing the curvature to the saturation of the magnetic moment at low temperature and high fields. In either case, the ratio of Ni^{3+} to total nickel is roughly 0.1%.

IV. SUMMARY

The magnetic properties of the Ca–Ni–K–(C–)O mixtures are surprisingly variable. Two of the samples

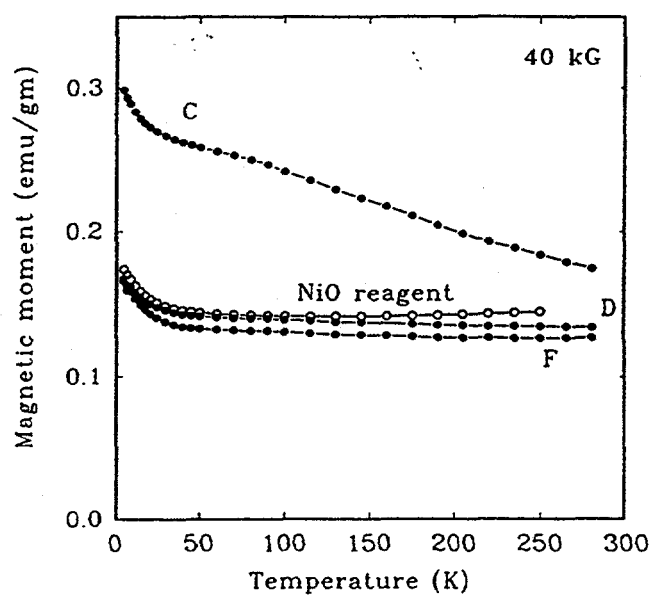

FIG. 5. Magnetic moment versus temperature for NiO reagent powder and samples C, D, and F, at 40 kG. Data for NiO were scaled for comparison with the other samples, as discussed in the text. Sample E (not shown) was similar to D and F.

TABLE II. Magnetic moment (emu/gm) at 40 kG and 280 K. The second column is normalized to the mass of NiO, computed from sample composition.

Sample	Moment per gm	Moment per gm of NiO
A	0.28	1.23
B	0.74	3.30
C	0.18	0.53
D	0.134	0.41
E	0.134	0.41
F	0.127	0.39
NiO	0.47	0.47

were particularly magnetic, and the plots of magnetic moment were markedly nonlinear as functions of the applied magnetic field. These samples contained calcium carbonate. From the magnetic properties alone, elemental ferromagnetic nickel is believed to be present, an expectation that was confirmed by x-ray diffraction. Doping with potassium increased the amount of Ni^0. The other four samples had magnetic properties that are attributed entirely to small NiO particles, with susceptibility increasing with decreasing particle size (decreasing calcination temperature). The sample treated at 485 °C was superparamagnetic, with twice the magnetism at low temperatures as NiO reagent. A T^{-1} peak in magnetic moment seen below 50 K in all samples may be due to Ni^{3+} ions.

The presence of nickel metal in NiO samples is readily detected magnetically by the large magnetic moment, large initial susceptibility, and saturation at low applied magnetic fields.

ACKNOWLEDGMENTS

This work was supported by the United States Department of Energy under Contract DE-AC03-76SF00098 and the Assistant Secretary for Fossil Energy, Office of Technical Coordination, through the Morgantown Energy Technology Center, Morgantown, West Virginia 26505.

REFERENCES

1. P. Pereira, S.H. Lee, G.A. Somorjai, and H. Heinemann, Catal. Lett. 6, 255 (1990).
2. J. Rasko, P. Pereira, G.A. Somorjai, and H. Heinemann, Catal. Lett. 9, 395 (1991).
3. J. Rasko, G.A. Somorjai, and H. Heinemann, Appl. Catal. A, General 84, 57 (1992).
4. D.M. Ginter, E. Magni, G.A. Somorjai, and H. Heinemann, Catal. Lett. 16, 197 (1992).
5. Y.F. Chang, G.A. Somorjai, and H. Heinemann, J. Catal. 141, 713 (1993).
6. Y.F. Chang, G.A. Somorjai, and H. Heinemann, J. Catal. 142, 697 (1993).
7. X.L. Mao, D.L. Perry, and R.E. Russo, J. Mater. Res. 8, 2400 (1993).
8. C.P. Bean, J. Appl. Phys. 26, 1381 (1955).
9. I.S. Jacobs and C.P. Bean, in *Magnetism*, edited by G.T. Rado and H. Suhl (Academic Press, New York, 1963), Vol. III, p. 271.
10. J.I. Gittleman, B. Abeles, and S. Bozowski, Phys. Rev. B 9, 3891 (1974).
11. T. Furubayashi and I. Nakatani, Solid State Commun. 74, 821 (1990).
12. W. Gong, H. Li, Z. Zhao, and J. Chen, J. Appl. Phys. 69, 5119 (1991).
13. A. Mauger, M. Escorne, V. Paul-Boncour, A. Percheron-Guegan, J.C. Achard, and J. Barrault, J. Phys. Chem. 92, 6004 (1988).
14. M. Escorne, A. Mauger, V. Paul-Boncour, and A. Percheron-Guegan, Solid State Commun. 76, 757 (1990).
15. J.T. Richardson and W.O. Milligan, Phys. Rev. 102, 1289 (1956).
16. J.R. Singer, Phys. Rev. 104, 929 (1956).
17. L. Néel, Compt. Rend. Acad. Sci. 252, 4075 (1961); 253, 9, 203, 1286 (1961); 254, 598 (1962).
18. L. Néel, J. Phys. Soc. Jpn. 17, Suppl. B-I, 676 (1962).
19. J. Cohen, K.M. Creer, R. Pauthenet, and K. Srivastava, J. Phys. Soc. Jpn. 17, Suppl. B-I, 685 (1962).
20. W.J. Schuele and V.D. Deetscreek, J. Appl. Phys. 33, 1136 (1962).
21. S. Matsuo, S. Satou, M. Suzuki, M. Sano, and H. Nakano, Z. Phys. D–Atoms, Molecules, Clusters 18, 281 (1991).
22. J.T. Richardson, D.I. Yiagas, B. Turk, K. Forster, and M.V. Twigg, J. Appl. Phys. 70, 6977 (1991).
23. J.T. Richardson, B. Turk, M. Lei, and M.V. Twigg, Appl. Catal. 83, 87 (1992).
24. Ref. 9, Secs. 3–5.

III. **Extended Abstract** - 1994 Fall Meeting of the Materials Research Society, Boston, MA, *"Studies of Calcium-Nickel-Potassium Oxide Films by Synchrotron X-Ray Fluorescence Microscopy"*

STUDIES OF CALCIUM-NICKEL-POTASSIUM OXIDE FILMS BY SYNCHROTRON X-RAY FLUORESCENCE MICROSCOPY

[Proceed. Fall Meet. Mat. Res. Soc., 375, 000(1994).

D. L. PERRY, A. C. THOMPSON, R. E. RUSSO, AND X. L. MAO

Lawrence Berkeley Laboratory
University of California
Berkeley, CA 94720

ABSTRACT

The use of synchrotron x-ray fluorescence microscopy to study the composition and homogeneity of laser deposited films of calcium-nickel-potassium oxides is described. Experimental conditions for preparing the films are given, and the results are discussed with respect to the x-ray fluorescence data concerning the distribution of the three metals in the films.

INTRODUCTION

Quaternary metal oxides involving calcium, nickel, and potassium have been shown to be quite effective in the catalysis of coal gasification and methane coupling. The catalysts are synthesized by a variety of techniques, including thermal decomposition of the metal salts, high-temperature annealing of the mixed oxides, or high-temperature dehydration/heating of a mixture of the metal hydroxides. An inherent problem with these syntheses, however, is the the much higher boiling points of the calcium and nickel oxides relative to those of potassium oxides, resulting in the loss of potassium from the catalysts at higher temperatures that must be used to form the oxides from the starting materials. A major consequence of this problem is that it is extremely difficult to synthesize highly reproducible samples of the quaternary metal oxides using traditional, standard thermal techniques [1].

One approach to incorporating all three of the metal oxides into one phase is the use of laser ablation to prepare films [2,3] of the catalysts so that they may be used for coatings, smooth surfaces on which to conduct detailed studies of gas-solid interface reactions that are involved in catalytic processes, and other applications. The problem of dissimilar boiling points of the three metal oxides system is overcome, since the laser ablation process effects the volatization of all three components from the target simultaneously.

EXPERIMENTAL

Films of calcium-nickel-potassium oxide were fabricated by pulsed laser deposition as previously described [3]. Briefly, pellet targets made of appropriate mixtures of CaO, NiO, and KNO_3 and pressed at 20,000 PSI were subjected to a beam from a KrF excimer laser operated at 248 nm with a 350 mJ/pulse and a 5 Hz repetition rate. The pulsed laser deposition chamber used in the film fabrication was operated containing a 10 mTorr atmosphere of oxygen while the deposition was occurring, with the single crystal MgO(100) film substrate being held at 600 ^{o}C. The deposition time was 15 minutes, with the films being cooled to room temperature in the 10 mTorr atmosphere within 30 minutes. Energy dispersive x-ray analyses gave a normalized

composition of Ca = 58 %, Ni = 35 %, and K = 7 % for the film studied by x-ray fluorescence microscopy. X-ray photoelectron spectroscopy confirmed the presence of only the calcium-nickel-potassium oxide; no nitrogen phases (such as nitrides) introduced by use of the nitrate as a target material were detected, while x-ray diffraction showed that the films were composed of a previously unreported phase of calcium-nickel-potassium oxide.

The films were analyzed using the new x-ray fluorescence microprobe at the Advanced Light Source (ALS) at Lawrence Berkeley Laboratory as previously described [4,5]. The x-ray microprobe uses a white radiation beam from a bending magnet on the synchrotron. Figure 1 shows a schematic diagram of the system. A pair of multilayer-coated spherical mirrors in a Kirkpatrick-Baez configuration are used to focus and monochromate (with 10 % bandpass) the beam.

The focused beam spot intensity was 3 x 10^9 photons/second, the beam spot size was 2 μ x 3 μ, and the incident x-ray energy was 8.5 keV. The samples were scanned in several areas, with a step size of 5 μ and a counting time of 100 seconds.

RESULTS AND DISCUSSION

The elemental distribution of calcium, nickel, and potassium in the laser ablation-generated films studied here show the films to be mostly homogeneous with respect to the three elements. Figure 2 shows the elemental maps [Note the differences in the scales for each element.] of the films, with each element being evenly distributed, as evidenced by the mostly flat contours of the individual elemental maps. Several locations on the film indicate morphological discontinuities, these being the result of small particles that are always inherent to the surfaces of films generated by laser ablation. Too, there are some areas of elemental heterogeneity, such as small differences in the calcium concentration shown in Fig. 2. Fig. 3 gives an even better perspective of the homogeneity of the films, the elemental ratios of the metals being shown. The elemental ratios are generally consistent with homogeneity, but again there are some minor variations across the surfaces of the imaged areas.

The results here are highly illustrative of the concept of microheterogeneity vs. macrohomogeneity. While the films, which can be formed at sizes in the inches, do show small domains of varying elemental stoichiometry, they are.--for the most part--functioning homogeneous films for purposes of their various applications.

ACKNOWLEDGMENTS

This work was supported under Contract No. DE-AC03-76SF00098, the Assistant Secretary for Fossil Energy, Office of Technical Coordination, through the Morgantown Energy Technology Center, Morgantown, WV, 26505, and the Director, Office of Energy Research, Office of Basic Energy Sciences, Materials Sciences Division, all of the U. S. Department of Energy. The authors also wish to thank Rodney Malone for his continued support of this research.

REFERENCES

1. D. L. Perry, P. Berdahl, and C. Perrino, J. Mater. Res., **9**, 2993(1994).
2. D. L. Perry, X. L. Mao, and R. E. Russo, J. Mater. Res., **8**, 2400(1993).
3. X. L. Mao, D. L. Perry, and R. E. Russo, High Temp. Sci., *in press.*

4. A. C. Thompson, K. L. Chapman, G. E. Ice, C. J. Sparks, W. Yun, B. Lai, D. Legnini, P. J. Vicarro, M. L. Rivers, D. H. Bilderback, and D. J. Thiel, Nuclear Instruments and Methods in Physics Research, Section A, 319, 320(1992).
5. A. C. Thompson, K. L. Chapman, and J. H. Underwood, Optics for High-Brightness Synchrotron Beamlines, SPIE, 1740(1992).

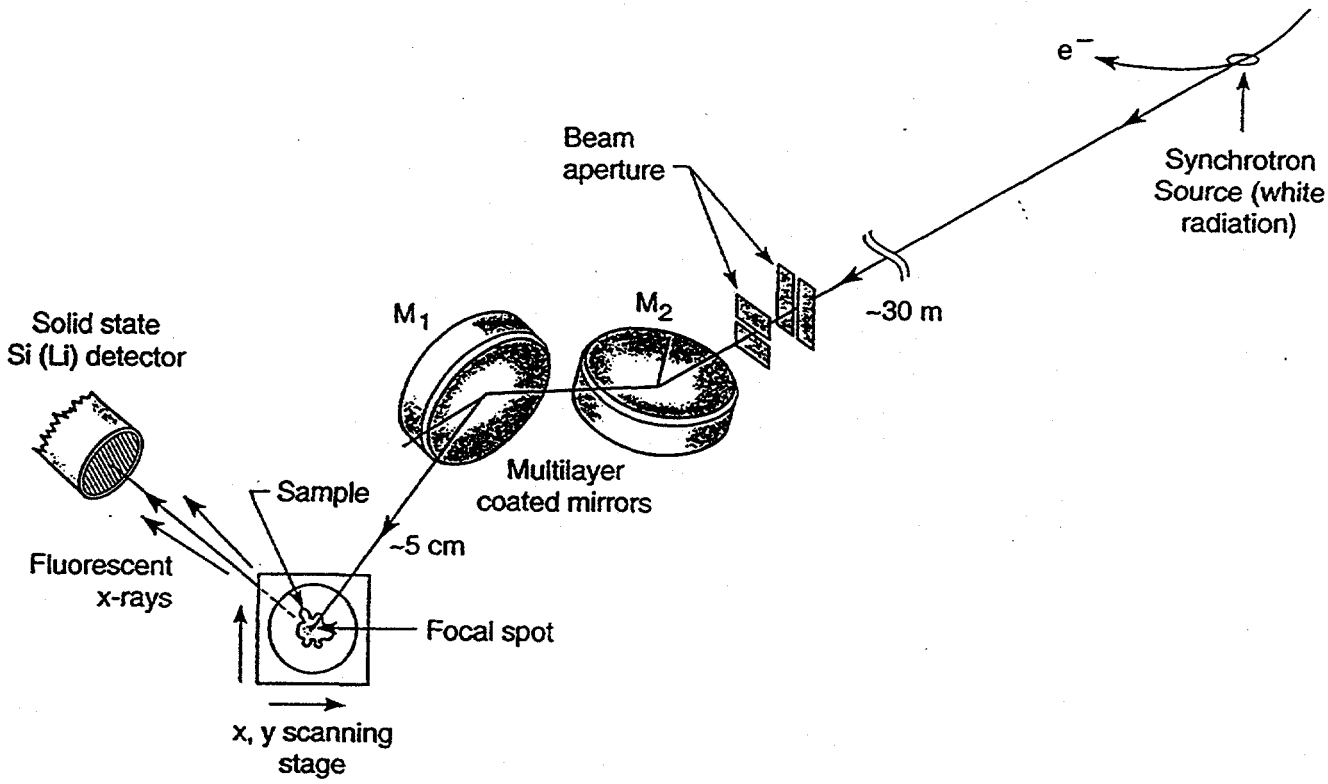

Figure 1. Experimental arrangement for the x-ray fluorescence microprobe facility (Beamline 10.3.1) at the Advanced Light Source (ALS) at Lawrence Berkeley Laboratory.

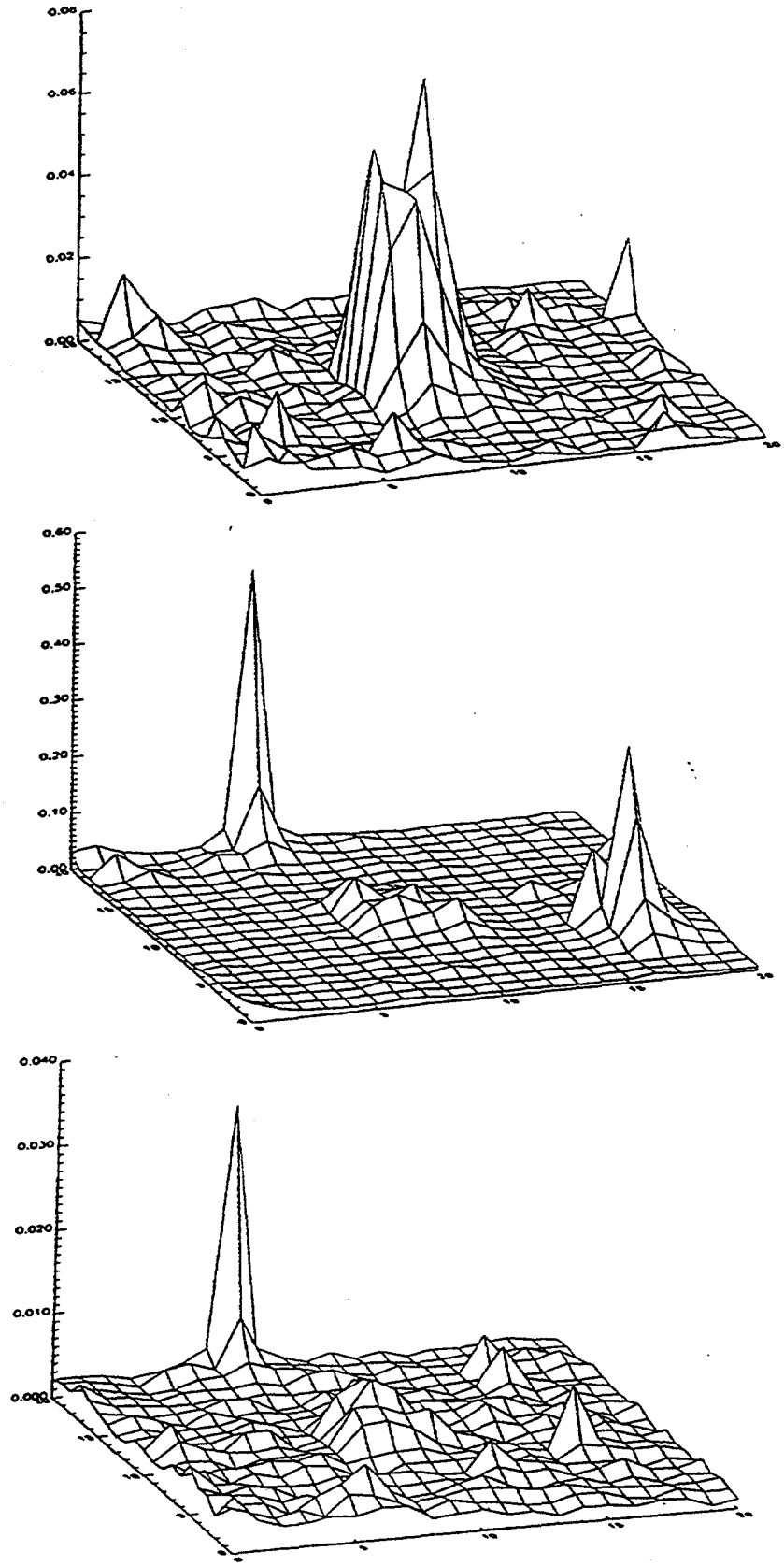

Figure 2. X-ray fluorescence microprobe elemental maps for calcium (top), nickel (middle), and potassium (bottom). The *x-y* plane of the shown image is 100 μ x 100 μ.

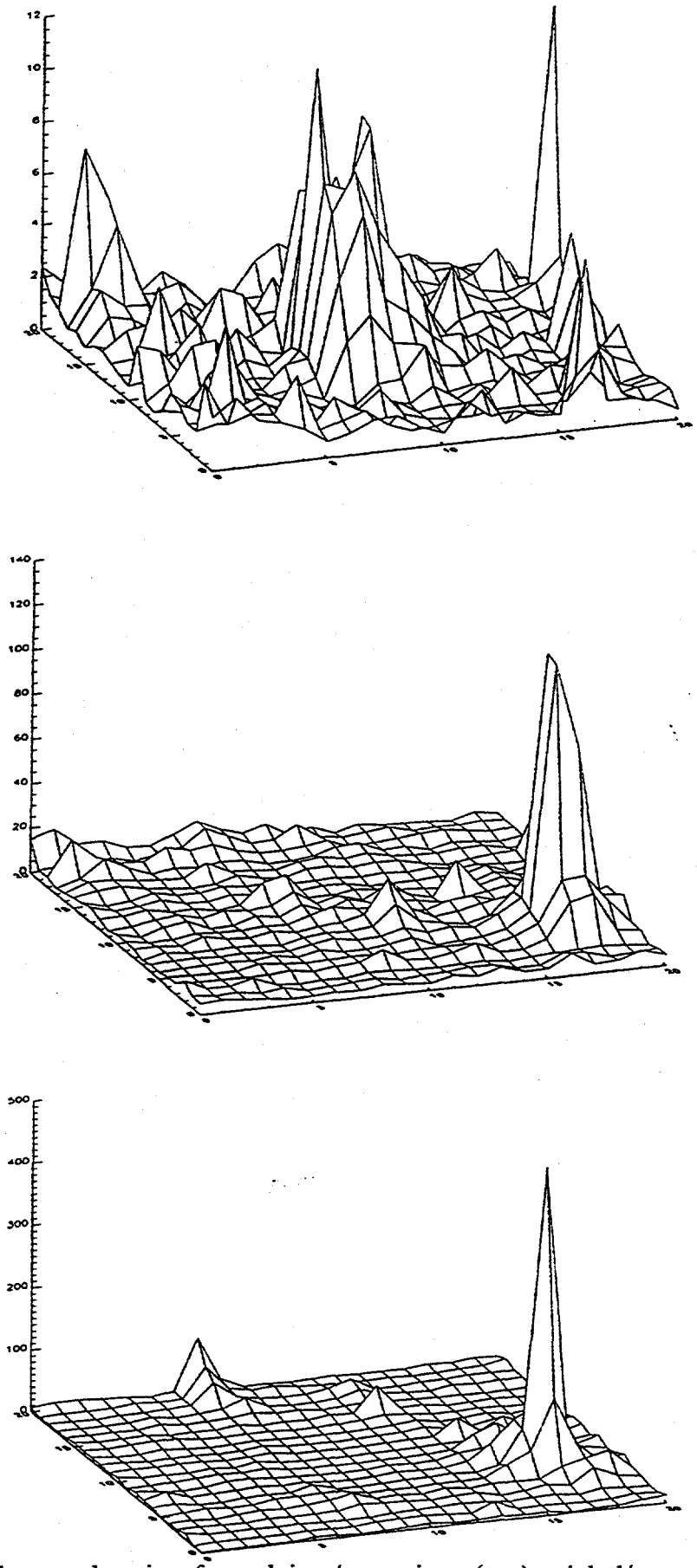

Figure 3. Elemental ratios for calcium/potassium (top), nickel/potassium (middle), and nickel/calcium (bottom) in the laser deposited films.